HHS Public Access

Author manuscript

Nat Cell Biol. Author manuscript; available in PMC 2018 December 25.

Published in final edited form as:

Nat Cell Biol. 2018 July ; 20(7): 775–781. doi:10.1038/s41556-018-0118-z.

Aspartate is a limiting metabolite for cancer cell proliferation under hypoxia and in tumors

Javier Garcia-Bermudez[1], **Lou Baudrier**[1], **Konnor La**[1], **Xiphias Ge Zhu**[1], **Justine Fidelin**[2], **Vladislav O Sviderskiy**[3], **Thales Papagiannakopoulos**[3], **Henrik Molina**[2], **Matija Snuderl**[3], **Caroline A. Lewis**[4], **Richard L. Possemato**[3], and **Kıvanç Birsoy**[1,*]

[1]Laboratory of Metabolic Regulation and Genetics, The Rockefeller University, 1230 York Avenue, New York, NY 10065, USA

[2]Proteomics Resource Center, The Rockefeller University, 1230 York Avenue, Box 105, New York, New York, 10065, USA

[3]Department of Pathology, New York University School of Medicine, New York, New York, 10016 USA

[4]Whitehead Institute for Biomedical Research, 9 Cambridge Center, Cambridge, MA 02142 USA

SUMMARY

As oxygen is essential for many metabolic pathways, tumor hypoxia may impair cancer cell proliferation (1–4). However, the limiting metabolites for proliferation under hypoxia and in tumors are unknown. Here, we assessed proliferation of a collection of cancer cells upon inhibition of the mitochondrial electron transport chain (ETC), a major metabolic pathway requiring molecular oxygen (5). Sensitivity to ETC inhibition varied across cell lines, and subsequent metabolomic analysis uncovered aspartate availability as a major determinant of sensitivity. Cell lines least sensitive to ETC inhibition maintain aspartate levels by importing it through an aspartate/glutamate transporter, SLC1A3. Genetic or pharmacologic modulation of SLC1A3 activity markedly altered cancer cell sensitivity to ETC inhibitors. Interestingly, aspartate levels also decrease under low oxygen, and increasing aspartate import by SLC1A3 provides a competitive advantage to cancer cells at low oxygen levels and in tumor xenografts. Finally, aspartate levels in primary human tumors negatively correlate with the expression of hypoxia markers, suggesting that tumor hypoxia is sufficient to inhibit ETC and, consequently, aspartate synthesis in vivo. Therefore, aspartate may be a limiting metabolite for tumor growth and aspartate availability could be targeted for cancer therapy.

Correspondence: kbirsoy@rockefeller.edu.

AUTHOR CONTRIBUTIONS

K.B. and J.G.B. conceived the project and designed the experiments. J.G.B. and L.B. performed most of the experiments. K.L. performed computational analysis. X.G.Z assisted with the immunofluorescence experiments. C.L., J.F. and H.M. performed metabolite profiling experiments. T.P. assisted with the mouse xenograft experiments. R.P., M.S. and V.O.S. provided human tumor data and analysis. K.B. and J.G.B wrote and edited the manuscript.

As solid tumors frequently outgrow their blood supply, cancer cells reside in nutrient and oxygen poor environments (6, 7). To sustain proliferation, cancer cells rewire their metabolic pathways and adapt to the tumor nutrient environment. In particular, low oxygen activates a transcriptional program that induces glucose uptake and glycolysis, while suppressing electron transport chain (ETC) activity (6, 8). However, the cellular effects of low oxygen extend beyond central glucose metabolism, as there are more than 145 metabolic reactions that employ molecular oxygen as an electron acceptor (9, 10). These oxygen-requiring reactions generate energy and provide critical building blocks including fatty acids, amino acids, cholesterol and nucleotides. Nonetheless, which of these cellular metabolites are limiting for cancer cell proliferation under hypoxia and in tumors remains poorly understood.

Among the oxygen requiring metabolic pathways, ETC activity provides a highly efficient route for eukaryotic cells to generate ATP (11). ETC inhibition suppresses cancer cell proliferation *in vitro* and *in vivo* (12, 13), but whether all cancer cells have similar sensitivity to ETC inhibition, and the precise metabolic determinants of this sensitivity are not clear. To address this question, we assessed proliferation of a collection of 28 patient-derived cancer cell lines derived from blood, stomach, breast, colon, and lung tumors, and measured the effect of ETC inhibition on cell proliferation (Fig. 1a). Given that inhibition of different complexes of the ETC may have pleiotropic effects on metabolism, we used inhibitors of complex I (piericidin), complex III (antimycin A), and complex V (oligomycin) as well as phenformin, an anti-diabetic drug that inhibits the ETC. Interestingly, cancer cell lines display diverse growth responses to ETC inhibition (Fig. 1a). While proliferation of many lines is strongly affected by ETC inhibitors, a subset was less sensitive or some were completely resistant to ETC inhibition. The sensitivity to inhibition of each ETC complex significantly correlated with the others, suggesting that the effect of ETC inhibition on proliferation is largely independent of the complex inhibited (Fig. 1a, Supplementary Fig. 1a). However, a subset of cancer cell lines exhibited sensitivity to ETC inhibition that was partially complex dependent. For example, the sensitivity profiles of complex I and III inhibition were more highly correlated with each other than with that of complex V inhibition, reflecting the distinct functions of complexes I/III and IV in the ETC. Similarly, the sensitivity profile of complex I inhibitor piericidin most strongly correlated with that of phenformin ($r = 0.90$, $P = 1.7e\text{-}11$) (Fig. 1b, Supplementary Fig. 1a), consistent with the previous findings that the major cellular target of anti-diabetic biguanides such as metformin and phenformin is complex I (14, 15).

Given these results, we hypothesized that fundamental differences in metabolic function might exist between cancer cell lines most sensitive (P12-ICHIKAWA, ALL-SIL, HPB-ALL, MV-4-11, A549, SU-DHL-8) and least sensitive (COLO-704, MDA-MB-157, NOMO-1, RPMI 8226, COLO 320DM, SNU-1) to ETC inhibition. To understand why a subset of cancer cell lines is less sensitive to ETC inhibition, we compared the effects of piericidin treatment on levels of key metabolites in the two groups (Fig. 1c). Even though ETC inhibition caused profound changes in the metabolism of all cancer cell lines, we were only able to detect significant differences in 19 metabolites between the two groups (Fig. 1c, Supplementary Fig. 1b). Among these were TCA cycle intermediates (malate, citrate, fumarate), nucleotides (UMP, ADP, UDP, CDP), and the amino acids aspartate and

argininosuccinate. Synthesis of aspartate is limiting for cancer cell proliferation when ETC is impaired (16, 17) and aspartate is a precursor for the synthesis of many of these metabolites including argininosuccinate and nucleotides. We therefore focused our attention on aspartate and asked whether the change in aspartate levels might determine the response to ETC inhibition. Indeed, among all amino acids, aspartate is the only one that drops substantially (~3 fold) in ETC inhibition sensitive cancer cell lines, while its levels are mostly maintained in the resistant counterparts (Fig. 1d). Therefore, our results strongly point to the change in aspartate levels as an important determinant of sensitivity to ETC inhibition across different cancer cells.

We next sought to understand how a subset of cancer cells could maintain aspartate levels under ETC inhibition and whether maintenance of aspartate levels decreases sensitivity to ETC inhibition. Cells can increase aspartate availability by (i) increasing de novo synthesis from oxaloacetate or (ii) importing aspartate from the extracellular environment. Remarkably, unlike ETC inhibition sensitive cells, the majority of ETC inhibition resistant cell lines (COLO-704, MDA-MB-157, NOMO-1, COLO 320DM, SNU-1) were naturally able to uptake extracellular ^{14}C-labeled aspartate (Fig. 2a, Supplementary Fig. 2a), arguing that increased aspartate transport may account for the observed resistance to ETC inhibition. Indeed, standard RPMI media lacking aspartate, but not the structurally similar glutamate, sensitizes otherwise resistant cancer cells displaying aspartate import to ETC inhibitors (Fig. 2b, Supplementary Fig. 2b). These results suggest that maintaining aspartate levels by import enables cancer cell proliferation under ETC inhibition.

Aspartate is a charged amino acid at physiological pH and requires the presence of specific transporters for cellular import (Supplementary Fig. 2c), as most mammalian cells cannot uptake aspartate from their environment (18). Expression of these known transporters is normally restricted to neuronal tissues (18). To identify the transporter(s) that import aspartate in ETC inhibition resistant cancer cell lines, we asked whether the expression of any particular transporter is most predictive of the response to ETC inhibition. Correlation of antimycin's effect on cell viability with transcriptome-wide mRNA expression data from the Cancer Cell Line Encyclopedia (CCLE) (19) revealed the aspartate/glutamate transporter *SLC1A3* as a top scoring gene ($r = 0.64$, $P = 2.9 \times 10^{-4}$) (Fig. 2c). Indeed, many of the cancer cell lines with detectable aspartate import activity express SLC1A3 protein (Fig. 2d). One exception to this correlation, COLO-704, expresses SLC1A2, a close homolog of SLC1A3, which is also capable of importing aspartate (Supplementary Figs 2d-e). Two additional resistant cell lines (RPMI-8226 and DU4475) do not import aspartate, suggesting the existence of alternative mechanisms to overcome ETC inhibition.

SLC1A3 is a glutamate-aspartate transporter localized on the plasma membrane (Supplementary Fig. 2f) and normally expressed in glial cells (20). However, SLC1A3 is also highly expressed in a subset of non-glial epithelial tumors and its genomic locus is significantly amplified (Supplementary Fig. 2g). To determine whether SLC1A3 expression is necessary for cancer cell proliferation under ETC inhibition, we used the CRISPR-Cas9 system and generated a clonal SLC1A3 knock out of the SNU-1 cell line (SLC1A3_KO), in which SLC1A3 is normally highly expressed (Fig. 2e). SLC1A3_KO cells take up 10 fold less aspartate and are more sensitive to piericidin and antimycin than wild type counterparts

(Fig. 2f-g). Importantly, expression of an sgSLC1A3-resistant human SLC1A3 cDNA in the null cells or addition of pyruvate, which facilitates aspartate synthesis despite ETC inhibition (21), completely restored resistance to ETC inhibitors (Fig. 2g). Small molecule inhibitors targeting SLC1A3 (TFB-TBOA and UCPH 101) effectively block aspartate/glutamate uptake (Fig. 2f)(22–24). These pharmacologic inhibitors of SLC1A3 sensitize SNU-1 cells and other ETC inhibition resistant cell lines with high SLC1A3 expression including those with SLC1A3 amplification (NCI-H596, SNU-182, Detroit-562) to ETC inhibitors (Fig. 2h, Supplementary Fig. 2h-i). Additionally, we found that overexpression of SLC1A3 in A549, a cell line with undetectable endogenous SLC1A3 expression, is sufficient to enable the aspartate uptake and the proliferation of these cells under ETC inhibition (Fig. 2i, Supplementary Fig. 2j). Taken together, these findings reveal that SLC1A3 expression permits cancer cell proliferation under ETC inhibition and that expression of the aspartate transporter, SLC1A3, is a predictor of the proliferative response to ETC inhibition.

Aspartate levels can be limiting for cell proliferation under pharmacologic inhibition of mitochondrial respiration (16, 17), but whether aspartate is a limiting metabolite under conditions relevant to tumor growth is not known. As cancer cells in tumors are often starved for oxygen due to dysfunctional vasculature, we hypothesized that insufficiency of oxygen likely restricts aspartate biosynthesis via impairing ETC function and redox balance (Supplementary Fig. 3a). To first test whether aspartate is depleted in hypoxia, we measured amino acid levels of A549 and PANC-1 cancer cells, which have no detectable SLC1A3 expression, in standard atmospheric oxygen conditions (21%) or in reduced oxygen similar to that found in hypovascularized tumors (0.5%) (25, 26). Hypoxia causes profound metabolic changes, particularly a 4-fold decrease in the levels of aspartate and asparagine, which is synthesized from aspartate (Fig. 3a, Supplementary Fig. 3b). These data raise the possibility that low aspartate levels can limit proliferation under low oxygen, similar to what we observed for ETC inhibition, and that increasing aspartate levels may also promote proliferation in hypoxia. To test this possibility, we expressed SLC1A3 in A549 and PANC-1 cell lines as well as counterparts derived from $Kras^{G12D}/p53^{-/-}$ driven lung and pancreas cancer mouse models (KP lung and KP pancreas). Expression of SLC1A3 in these four cancer cell lines raised aspartate levels and increased their proliferation rates in hypoxia (Fig. 3b-c). Improved proliferative capacity under hypoxia depends on the aspartate transport activity of SLC1A3 as aspartate depletion or inhibition of SLC1A3 with a small molecule inhibitor completely eliminates the rescue phenotype (Fig. 3c). While aspartate is present in standard RPMI media at a concentration of 150 uM, its concentration in human and mouse serum is much lower (10-30 uM) (Supplementary Fig. 3c) (27). However, culturing SLC1A3 expressing cancer cells in physiological aspartate concentrations (27) is still sufficient to enable proliferation under ETC inhibition or hypoxia (Supplementary Fig. 3e,f), validating that SLC1A3 is a high affinity transporter and can import aspartate at 20 uM, a concentration on par with the levels of aspartate found in circulation. Therefore, our data indicate that aspartate is a major limiting metabolite for optimal cell proliferation under hypoxia.

We next asked whether low aspartate is also a metabolic limitation for tumor growth *in vivo*. To test the role of aspartate availability in tumor growth, we performed a competitive

proliferation assay between vector and SLC1A3 infected A549 and KP lung cancer cells under hypoxia, pharmacologic ETC inhibition and as tumor xenografts. Indeed, exogenous expression of SLC1A3 provides a growth advantage compared to vector infected controls in hypoxia or upon ETC inhibition in culture, and in tumor xenografts (Fig. 3d, Supplementary Fig. 3d). Of note, SLC1A3-expressing tumors have 2-fold higher aspartate levels compared to wild type counterparts (Supplementary Fig. 3g). Aspartate limitation is not necessarily common to all cancers, as the growth advantage conferred by SLC1A3 expression was not observed in Kras mutant mouse pancreas tumors (Supplementary Fig. 3h). This suggests that some cancer types might meet their aspartate supply through alternative routes such as macropinocytosis *in vivo* (28, 29) (30). Collectively, our results provide evidence that aspartate can be a growth-limiting metabolite in tumors.

Aspartate is a proteinogenic amino acid but can also contribute to nucleotide synthesis and TCA cycle anaplerosis. To understand why aspartate is limiting for cancer cell proliferation under hypoxia, we measured the generation of key metabolites derived from isotope labeled aspartate in A549 and PANC-1 cells. Aspartate can be directly used as a substrate to replenish the TCA cycle via the action of aspartate transaminases, generating citrate with four 13C atoms (m+4) and malate with two 13C atoms (m+2). However, we observe only modest labeling of malate/fumarate (m+2) and citrate (m+4) from ^{13}C-aspartate in these cell lines (Supplementary Fig. 4a). Consistent with this observation, SLC1A3 expression does not increase oxygen consumption, which would be expected if aspartate supplementation substantially drove TCA flux (Supplementary Fig. 4b). We then focused our attention on the contribution of imported aspartate to nucleotide synthesis. In purine biosynthesis, aspartate acts as a nitrogen donor for both the purine ring and for the production of adenine from hypoxanthine. In pyrimidine biosynthesis, aspartate contributes three carbon atoms during the production of UMP and TMP via the intermediate orotate. Interestingly, 50 to 80% of orotate, dTMP and UMP in SLC1A3 expressing cells are derived from imported aspartate specifically under hypoxia and ETC inhibition, and only minimally under normoxic conditions (Fig. 3e, Supplementary Fig. 4a). Additionally, a significant portion of aspartate can contribute to purine synthesis as measured by [^{15}N]-Aspartate incorporation into AMP in SLC1A3-expressing cells (Fig. 3e, Supplementary Fig. 3c). We observed similar results even under physiological aspartate concentrations (Supplementary Fig. 4d). These observations raise the possibility that low aspartate levels might limit nucleotide production necessary for cell proliferation under hypoxia and ETC inhibition, conditions where de novo aspartate synthesis is inhibited. Remarkably, in 3 out of the 4 cell lines, nucleoside supplementation alone substantially rescued growth inhibition by hypoxia even in the absence of aspartate, consistent with the limiting role of nucleotide biosynthesis (Fig. 3f). Thus, our data argue that imported aspartate is a major source for nucleotide biosynthesis and that aspartate derived nucleotide synthesis is limiting for proliferation of a subset of cancer cells under hypoxia.

Given our results demonstrating that hypoxic cells are deficient in aspartate production, we asked whether aspartate could be a metabolic marker predicting the degree of hypoxia in primary human tumors. Hypoxia activates a specific transcriptional program through hypoxia inducible factors (31), which strongly induces transcription of genes related to metabolism and angiogenesis, most notably VEGFA, CA9 and HK2 (32). To test whether

tumor hypoxia impacts aspartate levels in glioblastomas, we collected 24 snap frozen glioblastomas for metabolomics and transcriptomic analyses and correlated mRNA expression of hypoxic markers with the abundance of individual metabolites. Remarkably, among 128 metabolites detected, steady state aspartate levels correlate significantly ($p<0.01$) with these established markers of tumor hypoxia (Fig. 4a, Supplementary Fig. 4e-f). Interestingly, steady state aspartate levels correlated with the hypoxic markers even more strongly than lactate and acylcarnitines, metabolites commonly viewed as being increased in hypoxic tumor regions (Fig. 4b) (33, 34). These results suggest that the degree of hypoxia experienced by human tumors may inhibit aspartate synthesis through ETC inhibition, making aspartate a metabolite marker for tumor hypoxia in glioblastomas.

Our data are consistent with a model whereby tumor hypoxia limits ETC function, blocking aspartate availability and nucleotide biosynthesis (Fig. 4c). Similar to our results, heterologous expression of a guinea pig asparaginase also increases aspartate availability and tumor growth (35). Consistent with this observation, the degree of ETC inhibition present in primary human tumors is sufficient to limit aspartate production, as hypoxic markers correlate with aspartate levels. While low aspartate levels may restrict tumor growth by impacting protein and nucleotide synthesis, nucleotide supplementation alone can restore proliferation of a subset of aspartate-limited cancer cells, implying differential metabolic needs of different cancer types under hypoxia. Finally, acquisition of the ability to import aspartate through upregulation of gene expression or genomic amplification of aspartate transporters may be an important metabolic adaptation for tumors that develop in or are selected by transient rounds of hypoxia. Our findings indicate that low oxygen levels may constrain *in vivo* tumor growth through aspartate limitation and pathways relevant to aspartate availability could thus be targeted for therapy in a subset of tumors.

MATERIAL AND METHODS

Cell lines, compounds and constructs

Antibodies to SLC1A3 (GTX20262, 1:1,000 for Western blot; 1:500 for immunofluorescence) and Beta-Actin (GTX109639, 1:10,000) were obtained from GeneTex; HRP-conjugated anti-rabbit antibody from Santa Cruz (sc-2357, 1:5,000); Alexa Fluor 488 donkey anti-rabbit antibody from Invitrogen (A-21206, 1:250); DAPI from Vector Laboratories; sodium pyruvate, polybrene, puromycin, thymidine, uridine, adenosine, cytidine and inosine from Sigma; aspartic acid from Acros; glutamic acid from Fisher Scientific; blasticidin from Invivogen; antimycin A and piericidin from Enzo Life Sciences; oligomycin from EMD Millipore; phenformin from Fluka; TFB-TBOA and UCPH 101 from Tocris; and Matrigel from Corning.

Identities of all the cell lines used in this study were authenticated by Single Tandem Repeat (STR) profiling. Among all the cell lines, 3 of them were in ICLAC as misidentified cell lines but included in our analysis for diversity due to their oncogene status and metabolic phenotypes: RPMI-8402 is an asparagine auxotroph leukemia cell line, U-937 a rare histiocytic lymphoma cell line, and HPB-ALL is a cell line with Notch activating mutations. Identities of these cell lines were authenticated by STR profiling (Supplementary Fig. 1c). Cell lines were cultured in RPMI medium containing 1 mM glutamine, 10% fetal bovine

serum, penicillin and streptomycin. For proliferation assays under aspartate and glutamate depletion and for tracing experiments, RPMI without amino acids (US Biologicals-R8999) was used, supplemented with individual amino acids at RPMI concentrations. For oxygen consumption experiments, assay media consisted of RPMI media with L-glutamine and without sodium bicarbonate (Corning, 50-020-PC). Dialyzed serum used in aspartate and glutamate depletion experiments was prepared using Dialysis Tubing (Fisher Scientific) and fetal bovine serum (Sigma). For tracing experiments, [U-^{13}C]-L-Aspartic acid (CIL, CLM-1801-H) and L-Aspartic Acid-15N (CIL, NLM-718-0.5) were used. [^{14}C(U)]-L-Aspartic acid (Moravek, MC139) was used for aspartate uptake assays.

Generation of the lentiviral sgSLC1A3 was achieved via ligation of hybridized oligos (below) into lentiCRISPR-v1 vector linearized with BsmBI by ligation (NEB). sgSLC1A3_5F, caccgCAAGTACTTCTCCTTTCCTG; sgSLC1A3_5R, aaacCAGGAAAGGAGAAGTACTTGc. Mutagenesis by PCR-overlap extension and Gibson assembly was used for sgRNA resistant SLC1A3 cDNA generation.

The primers used for the two PCR reactions with the previously generated PMXS-ires-blast-SLC1A3 as a template are below: SLC1A3_F, GCCGGATCTAGCTAGTTAATTAAGCCACCATGACTAAAAGCAATGGAGAAGAGCCC; SLC1A3-gRes_R, CATCCTCATCAGAAGTTCACCGGGGAAGGAGAAGTACTTGACTTC; SLC1A3-gRes_F, GAAGTCAAGTACTTCTCCTTCCCCGGTGAACTTCTGATGAGGATG; SLC1A3_R, GGGCGGAATTTACGTAGCCTACATCTTGGTTTCACTGTCGATGGG.

Proliferation Assays

Cell lines were cultured in 96-well plates at 1,000 cells per well in a final volume of 0.2 ml RPMI-1640 media (Corning) under the indicated treatments. For adherent cells, drugs were added 2 hours after plating. An initial time point of untreated cells was used for normalization. After 5 days of growth, 40 μl of Cell Titer Glo reagent (Promega) was added and luminescence was read using a SpectraMax M3 plate reader (Molecular Devices). Data is presented as fold change in luminescence relative to the mean final luminescence of untreated cells. For aspartate and glutamate depletion, a custom RPMI media without amino acids (US biologicals) supplemented with 10% dialyzed FBS was used by adding all the amino acids except for aspartate, glutamate and asparagine (supplemented with 150 uM aspartate or glutamate when indicated).

Cell Counting Assays

Cell lines were plated in 6-well plates at 1,000-5,000 cells per well in standard conditions (normoxia) and in a hypoxia chamber (INVIVO) set to 0.5% O_2. For hypoxic conditions, culture media were pre-incubated for 24 h. After 5 days of growth, cells were trypsinized and counted using a Beckman Z2 Coulter Counter with a size selection setting of 8–30 um.

Aspartate Uptake

Adherent cells were plated in 6-well plates at 200,000 cells per well 24 h prior to the assay. Each well was then washed three times before the uptake experiment with Hank’s Balanced

Solution (HBSS, Invitrogen). For suspension cell lines, 500,000 cells were pelleted by centrifugation and washed three times with HBSS. Uptake assays were done in 1 mL of HBSS supplemented with 5 mM HEPES and 2 mM Glucose and the kinetic measurement at 37°C was initiated by adding 0.1 μCi of L-Aspartic acid [^{14}C(U)] per well. An initial reference value was taken for every cell line by washing away the labeled aspartate after addition of 1 mL of cold HBSS buffer supplemented with 150 μM of unlabeled L-aspartate. After 10 min of assay, the same procedure for stopping the reaction was used both for adherent (three washes per well) or suspension cells (centrifugation of cells in 1.5 ml tube at 3,000 rpm and three consecutive washes), prior to lysis in 400 μL of lysis buffer (0.1 N NaOH and 0.01% SDS) for 10 min at room temperature. 50 μL of cell lysate was used for protein quantification and the remaining 350 μL was mixed in scintillation vials with 5 mL of ScintiSafe Econo Cocktail (Fisher). Radioactivity was measured in a Tri-Carb 2910 Liquid Scintillation Analyzer (Perkin Elmer) and the counts per minute (cpm) for each vial were normalized by microgram of protein and presented as relative to the initial time point.

Generation of Knockout and cDNA Overexpression Cell Lines

sgRNA targeting SLC1A3 (GCAAGTACTTCTCCTTTCCTG) was cloned into lentiCRISPR-v1 linearized with BsmBI by ligation (NEB). Lentiviral vector expressing the sgRNA was transfected into HEK293T cells with lentiviral packaging vectors VSV-G and Delta-VPR using XtremeGene transfection reagent (Roche). For overexpression of aspartate transporters, retroviral vectors with indicated cDNAs were transfected along with retroviral packaging plasmids (Gag-pol and VSV-G) to HEK293T cells. 48 hr after transfection, virus particles were collected and filtered using a 0.45 mm filter to eliminate cells. Target cells were plated in 6-well tissue culture plates and infected in media containing the virus and 8 mg/ml of polybrene. To increase transduction efficiency, a spin infection was performed by centrifugation at 2,200 rpm for 1.5 hr. 48 hr after the infection, selection of transduced cells was performed by addition of puromycin (for sgRNA lentiviral vector) or blasticidin (for overexpression retroviral vectors). For SLC1A3-knockout cells, cells were single-cell isolated by serial dilution into a 96-well plate containing 0.1 mL of media. Single cell clones were grown for three weeks, and the resultant SLC1A3 $^{-/-}$ clones were validated by western blot and expanded.

Metabolite Profiling and Isotope Tracing

For the initial metabolite profiling experiment in resistant and sensitive lines, each indicated cell line (1.5 million cells per replicate) was cultured as triplicates in 6-well plates and treated for 8 hours with piericidin (10 nM). For aspartate tracing experiments in A549 and PANC-1 cell lines, 150,000 cells per well were pretreated with 10 nM piericidin or preincubated at 0.5% oxygen, as well as in RPMI without piericidin and at 21% oxygen. After 12 h, media was changed and replaced with 2 ml of custom RPMI media lacking aspartate, glutamate and asparagine and supplemented with [U-^{13}C]-L-Aspartate (150 uM or 20 uM) or [^{15}N]-L-Aspartate (150 uM or 20 uM) under indicated treatments for an additional 24 h. Cells were washed three times with 1 mL of cold 0.9% NaCl, and polar metabolites were extracted in 1 mL of cold 80% methanol containing internal standards (MSK-A2-1.2, Cambridge Isotope Laboratories, Inc.). After extraction, samples were nitrogen-dried and stored at −80C until analysis by LC-MS. Analysis was conducted on a

QExactive benchtop orbitrap mass spectrometer equipped with an Ion Max source and a HESI II probe, which was coupled to a Dionex UltiMate 3000 UPLC system (Thermo Fisher Scientific, San Jose, CA). External mass calibration was performed using the standard calibration mixture every 7 days.

Dried polar samples were resuspended in 100 μL water and 2 μL were injected into a ZIC-pHILIC 150 × 2.1 mm (5 μm particle size) column (EMD Millipore). Chromatographic separation was achieved using the following conditions: Buffer A was 20 mM ammonium carbonate, 0.1% ammonium hydroxide; buffer B was acetonitrile. The column oven and autosampler tray were held at 25°C and 4°C, respectively. The chromatographic gradient was run at a flow rate of 0.150 mL/min as follows: 0–20 min.: linear gradient from 80% to 20% B; 20–20.5 min.: linear gradient from 20% to 80% B; 20.5–28 min.: hold at 80% B. The mass spectrometer was operated in full-scan, polarity switching mode with the spray voltage set to 3.0 kV, the heated capillary held at 275°C, and the HESI probe held at 350°C. The sheath gas flow was set to 40 units, the auxiliary gas flow was set to 15 units, and the sweep gas flow was set to 1 unit. The MS data acquisition was performed in a range of 70–1000 m/z, with the resolution set at 70,000, the AGC target at 10e6, and the maximum injection time at 20 msec. Relative quantitation of polar metabolites was performed with XCalibur QuanBrowser 2.2 (Thermo Fisher Scientific) using a 5 ppm mass tolerance and referencing an in-house library of chemical standards. For stable isotope tracing studies, fractional labeling was corrected for natural abundance using an in-house algorithm, based on that discussed in Buescher et al.[1]. Metabolite levels were normalized to the total protein amount for each condition.

Oxygen consumption measurements

Oxygen consumption of intact cells was measured using an XF96 Extracellular Flux Analyzer (Seahorse Bioscience). For adherent cell lines (A549, KP Lung and KP Pancreas), 15,000 cells were plated 12 h prior to the assay using RPMI 8226 (Corning #50-020-PC) assay media as previously described[2]. Basal oxygen consumption measurements were normalized by protein levels.

Determination of NAD^+/NADH ratios

For measurement of NAD^+/NADH, manufacturer instructions for NAD/NADH Glo Assay were followed (Promega) with addition of previously reported modifications to the protocol[3]. Cells were incubated at 21% and 0.5% O_2 24 hr prior to being trypsinized and plated at a confluence of 400.000 cells/well in triplicates. After 24 hr incubation, cells were lysed in cold DTAB lysis buffer (1% Dodecyltrimethylammonium bromide in 0.2 N NaOH diluted 1:1 in PBS). Briefly, to measure NADH, a portion of the extracts were heated to 75C for 30 min in a basic lysis buffer. For NAD^+ measurement, samples were further diluted 1:1 with 0.4 N HCl and heated to 60C for 15 min, with the acidic conditions of this incubation degrading NADH. After quenching both reactions by addition of 0.25 M Tris, 0.2N HCl (NADH reaction) or 0.5M Tris base (NAD^+ reaction), manufacturer instructions to measure NAD^+/NADH were followed.

Immunoblotting

Cell pellets were washed twice with ice-cold PBS and lysed in a standard lysis buffer (10 mM Tris-Cl pH 7.5, 150 NaCl, 1 mM EDTA, 1% Triton X-100, 2% SDS, 0.1% CHAPS) supplemented with protease inhibitors (Roche). After sonication of each cell lysate and centrifugation for 10 min at 20,000 g, supernatants were collected and protein concentrations were determined by using Pierce BCA Protein Assay Kit (Thermo Scientific) with bovine serum albumin as a protein standard. Samples were then resolved on a 12% SDS-PAGE gel and analyzed as described[2].

Cell Mixing Competition Assays

Each indicated cell line transduced with control vector and expressing SLC1A3 cDNA was trypsinized and mixed in equal proportion. An initial sample of this mix was collected for further normalization. The mixed population of both lines was then cultured in RPMI media or custom media with varying concentrations of aspartate, in the presence of 30 nM Antimycin A, 10 nM Piericidin or subjected to growth at 0.5% O_2 in a hypoxic chamber for 14 days, by splitting every 3 days. Same cell mix was injected subcutaneously to NOD/SCID-gamma mice and tumors were grown for the same period of time. Genomic DNA was isolated from initial samples, cells cultured under different conditions in vitro, and the tumors collected from mice using the Blood and Tissue Kit (Qiagen) following the manufacturer's protocol. qPCR reactions were assayed on an ABI Real Time PCR System (Applied Byosystems) using SYBR Green Mastermix (Applied Biosystems) and the following primers: a common forward primer targeting the vector (GGTGGACCATCCTCTAGACT) and reverse primers either targeting the vector (GCAGGAATTCCCGTACCAC) or SLC1A3 cDNA (CATCTTGGGCTCTTCTCCATT).

Immunofluorescence

For immunofluorescence assays, cells were seeded on coverslips previously coated with fibronectin. Cells were then fixed for 15 min with 4% paraformaldehyde diluted in PBS at room temperature. After three washes with PBS, cells were permeabilized and treated with 0.01% Triton X-100 in PBS for 5 min prior to three extra PBS washes. After incubation with a blocking solution (5% normal donkey serum (NDS) in PBS) for 1 hour, coverslips were incubated with SLC1A3 primary antibody (GTX20262, 1:500 in blocking solution) for an additional hour, and washed 3 times with PBS. Secondary Alexa Fluor 488 donkey anti-rabbit antibody was diluted in blocking solution (1:250) and added to the coverslips for 45 min at room temperature, prior to three washes with PBS. Coverslips were then incubated with a 200 nM solution of DAPI in PBS for 5 min and mounted onto slides with Prolong Gold antifade mounting media (Invitrogen). Images were taken on a Delta Vision bright-field fluorescence Inverted Olympus IX-71 microscope (GE Healthcare).

Mouse studies

All animal studies and procedures were conducted according to a protocol approved by the Institutional Animal Care and Use Committee (IACUC) at the Rockefeller University. All mice were maintained on a standard light-dark cycle with food and water ad libitum. Xenograft tumors were initiated by injecting 1.5 million cells/100 uL of 30% Matrigel

subcutaneously. After injections in the left and right flanks of male and female 6-9 weeks old NOD/SCID gamma (NSG) mice (Jackson labs), tumors were grown for 14 days. For *in vivo* metabolite profiling experiments, 1.5 million cells of A549 cells expressing SLC1A3 or a control vector were injected subcutaneously in opposite flanks of NSG mice and grown for 14 days prior to the experiment. Animals were sacrificed and tumors were extracted and immediately lysed in cold 80% methanol containing internal standards by using a Bead Ruptor 24 (Omni International) by 6 cycles of 20 s at 6 m/s. Supernatants were collected after 10 min centrifugation at 10,000 × g, nitrogen dried and analyzed.

Primary Tumor Samples

Fresh frozen glioblastoma human primary tumor samples (24 IDH WT glioblastomas, Age: Min = 29, Max = 84, median = 65; 12 Male, 12 Female) were obtained for metabolomics and RNAseq using standard protocols. The tissues were homogenized in methanol/chloroform solution and separated into non-polar and polar fractions. Dried polar fractions were then analyzed for metabolomics analysis and normalized by total amino acid signal as described above. Tumor tissues were obtained from the archives of the Department of Neuropathology New York University (NYU) Langone Health after Institutional Review Board (IRB# i14-00948) approval and the study is compliant with relevant ethical regulations. Informed consent was obtained from all participants. All specimens were reviewed and classified according to the World Health Organization (WHO) classification by a board certified neuropathologist to confirm histological diagnosis and select blocks for molecular analysis.

Statistics & Reproducibility

GraphPad PRISM 7 and Microsoft Excel 15.21.1 software were used for statistical analysis. Error bars, P values and statistical tests are reported in the figure legends. All experiments (except metabolite profiling and RNA-seq data of primary tumor samples in Fig. 4 and Supp. Fig. 4e-f, which were done once) were performed at least 2 times with similar results. Both technical and biological replicates were reliably reproduced.

Data Availability

Deep-sequencing (RNA–seq) data that support the findings of this study have been deposited in the Gene Expression Omnibus (GEO) under accession code GSE113474. Metabolomics data of primary tumor samples (Fig. 4 and Supplementary Fig. 4e-f) have been deposited in Figshare (10.6084/m9.figshare.6167711). Source data for metabolite profiling experiments shown in Fig. 1, 3, and Supplementary Fig. 1, 4 have been provided as Supplementary Table 1. Correlation analysis for Figure 4 is provided as Supplementary Table 2. All other data supporting the findings of this study are available from the corresponding author on reasonable request.

Supplementary Material

Refer to Web version on PubMed Central for supplementary material.

Acknowledgments

We thank all members of the Birsoy lab for helpful suggestions; C. Moraes, and I.F.M. de Coo for providing WT 143B and CYTB 143B cell lines. KP cell lines are gifts from Nabeel Bardeesy and Thales Papagiannakopoulos. We also thank Aaron M. Hosios for natural abundance correction. This research is supported by an EMBO Long term fellowship to JGB (EMBO ALTF 887-2016). Profiling of human glioblastoma samples was supported by the Friedberg Charitable Foundation and Sohn Foundation grants to M.S. and Rachel Molly Markoff Foundation grant to M.S. and R.P. R.P. was supported by the NIH (R21CA198543), KB was supported by K22 (1K22CA193660), DP2 (DP2 OD024174-01), Irma-Hirschl Trust, AACR NextGen Grant, Breast Cancer Research Foundation and is a Searle Scholar, Sidney Kimmel Scholar and Basil O'Connor Scholar of March of Dimes.

References

1. Henze AT, et al. Loss of PHD3 allows tumours to overcome hypoxic growth inhibition and sustain proliferation through EGFR. Nature communications. Nov 25.2014 5:5582.
2. Goda N, et al. Hypoxia-inducible factor 1alpha is essential for cell cycle arrest during hypoxia. Molecular and cellular biology. Jan.2003 23:359. [PubMed: 12482987]
3. Durand RE, Raleigh JA. Identification of nonproliferating but viable hypoxic tumor cells in vivo. Cancer research. Aug 15.1998 58:3547. [PubMed: 9721858]
4. Webster L, Hodgkiss RJ, Wilson GD. Cell cycle distribution of hypoxia and progression of hypoxic tumour cells in vivo. British journal of cancer. 1998; 77:227. [PubMed: 9460993]
5. Chandel N, Budinger GR, Kemp RA, Schumacker PT. Inhibition of cytochrome-c oxidase activity during prolonged hypoxia. The American journal of physiology. Jun.1995 268:L918. [PubMed: 7611433]
6. Ackerman D, Simon MC. Hypoxia, lipids, and cancer: surviving the harsh tumor microenvironment. Trends in cell biology. Aug.2014 24:472. [PubMed: 24985940]
7. Pavlova NN, Thompson CB. The Emerging Hallmarks of Cancer Metabolism. Cell metabolism. Jan 12.2016 23:27. [PubMed: 26771115]
8. Semenza GL. Oxygen-dependent regulation of mitochondrial respiration by hypoxia-inducible factor 1. The Biochemical journal. Jul 01.2007 405:1. [PubMed: 17555402]
9. Goldfine H. The evolution of oxygen as a biosynthetic reagent. The Journal of general physiology. Sep.1965 49(Suppl):253.
10. Gardner LB, et al. Hypoxia inhibits G1/S transition through regulation of p27 expression. The Journal of biological chemistry. Mar 16.2001 276:7919. [PubMed: 11112789]
11. Enriquez JA, et al. Human mitochondrial genetic system. Rev Neurol. Apr.1998 26(Suppl 1):S21. [PubMed: 9810587]
12. Weinberg F, et al. Mitochondrial metabolism and ROS generation are essential for Kras-mediated tumorigenicity. Proceedings of the National Academy of Sciences of the United States of America. May 11.2010 107:8788. [PubMed: 20421486]
13. Weinberg SE, Chandel NS. Targeting mitochondria metabolism for cancer therapy. Nature chemical biology. Jan.2015 11:9. [PubMed: 25517383]
14. Wheaton WW, et al. Metformin inhibits mitochondrial complex I of cancer cells to reduce tumorigenesis. eLife. May 13.2014 3:e02242. [PubMed: 24843020]
15. Owen MR, Doran E, Halestrap AP. Evidence that metformin exerts its anti-diabetic effects through inhibition of complex 1 of the mitochondrial respiratory chain. The Biochemical journal. Jun 15.2000 348(Pt 3):607. [PubMed: 10839993]
16. Birsoy K, et al. An Essential Role of the Mitochondrial Electron Transport Chain in Cell Proliferation Is to Enable Aspartate Synthesis. Cell. Jul 30.2015 162:540. [PubMed: 26232224]
17. Sullivan LB, et al. Supporting Aspartate Biosynthesis Is an Essential Function of Respiration in Proliferating Cells. Cell. Jul 30.2015 162:552. [PubMed: 26232225]
18. Kanai Y, et al. The SLC1 high-affinity glutamate and neutral amino acid transporter family. Molecular aspects of medicine. Apr-Jun;2013 34:108. [PubMed: 23506861]
19. Barretina J, et al. The Cancer Cell Line Encyclopedia enables predictive modelling of anticancer drug sensitivity. Nature. Mar 28.2012 483:603. [PubMed: 22460905]

20. Storck T, Schulte S, Hofmann K, Stoffel W. Structure, expression, and functional analysis of a Na(+)-dependent glutamate/aspartate transporter from rat brain. Proceedings of the National Academy of Sciences of the United States of America. Nov 15.1992 89:10955. [PubMed: 1279699]

21. King MP, Attardi G. Human cells lacking mtDNA: repopulation with exogenous mitochondria by complementation. Science. Oct 27.1989 246:500. [PubMed: 2814477]

22. Tsukada S, Iino M, Takayasu Y, Shimamoto K, Ozawa S. Effects of a novel glutamate transporter blocker, (2S, 3S)-3-[3-[4-(trifluoromethyl)benzoylamino]benzyloxy]aspartate (TFB-TBOA), on activities of hippocampal neurons. Neuropharmacology. Mar.2005 48:479. [PubMed: 15755476]

23. Canul-Tec JC, et al. Structure and allosteric inhibition of excitatory amino acid transporter 1. Nature. Apr 27.2017 544:446. [PubMed: 28424515]

24. Abrahamsen B, et al. Allosteric modulation of an excitatory amino acid transporter: the subtype-selective inhibitor UCPH-101 exerts sustained inhibition of EAAT1 through an intramonomeric site in the trimerization domain. The Journal of neuroscience : the official journal of the Society for Neuroscience. Jan 16.2013 33:1068. [PubMed: 23325245]

25. Vaupel P, Kallinowski F, Okunieff P. Blood flow, oxygen and nutrient supply, and metabolic microenvironment of human tumors: a review. Cancer research. Dec 01.1989 49:6449. [PubMed: 2684393]

26. Vaupel P, Schlenger K, Knoop C, Hockel M. Oxygenation of human tumors: evaluation of tissue oxygen distribution in breast cancers by computerized O2 tension measurements. Cancer research. Jun 15.1991 51:3316. [PubMed: 2040005]

27. Cantor JR, et al. Physiologic Medium Rewires Cellular Metabolism and Reveals Uric Acid as an Endogenous Inhibitor of UMP Synthase. Cell. Apr 06.2017 169:258. [PubMed: 28388410]

28. Kamphorst JJ, et al. Human pancreatic cancer tumors are nutrient poor and tumor cells actively scavenge extracellular protein. Cancer research. Feb 01.2015 75:544. [PubMed: 25644265]

29. Commisso C, et al. Macropinocytosis of protein is an amino acid supply route in Ras-transformed cells. Nature. May 30.2013 497:633. [PubMed: 23665962]

30. Davidson SM, et al. Direct evidence for cancer-cell-autonomous extracellular protein catabolism in pancreatic tumors. Nature medicine. Feb.2017 23:235.

31. Wang GL, Jiang BH, Rue EA, Semenza GL. Hypoxia-inducible factor 1 is a basic-helix-loop-helix-PAS heterodimer regulated by cellular O2 tension. Proceedings of the National Academy of Sciences of the United States of America. Jun 06.1995 92:5510. [PubMed: 7539918]

32. Poon E, Harris AL, Ashcroft M. Targeting the hypoxia-inducible factor (HIF) pathway in cancer. Expert reviews in molecular medicine. Aug 27.2009 11:e26. [PubMed: 19709449]

33. Frezza C, et al. Metabolic profiling of hypoxic cells revealed a catabolic signature required for cell survival. PloS one. 2011; 6:e24411. [PubMed: 21912692]

34. Chughtai K, Jiang L, Greenwood TR, Glunde K, Heeren RM. Mass spectrometry images acylcarnitines, phosphatidylcholines, and sphingomyelin in MDA-MB-231 breast tumor models. Journal of lipid research. Feb.2013 54:333. [PubMed: 22930811]

35. Sullivan L, et al. Evidence for aspartate as an endogenous metabolic limitation for tumour growth. Nature Cell Biology. this issue.

1. Buescher JM, et al. A roadmap for interpreting (13)C metabolite labeling patterns from cells. Current opinion in biotechnology. 2015; 34:189–201. [PubMed: 25731751]

2. Birsoy K, et al. Metabolic determinants of cancer cell sensitivity to glucose limitation and biguanides. Nature. 2014; 508:108–112. [PubMed: 24670634]

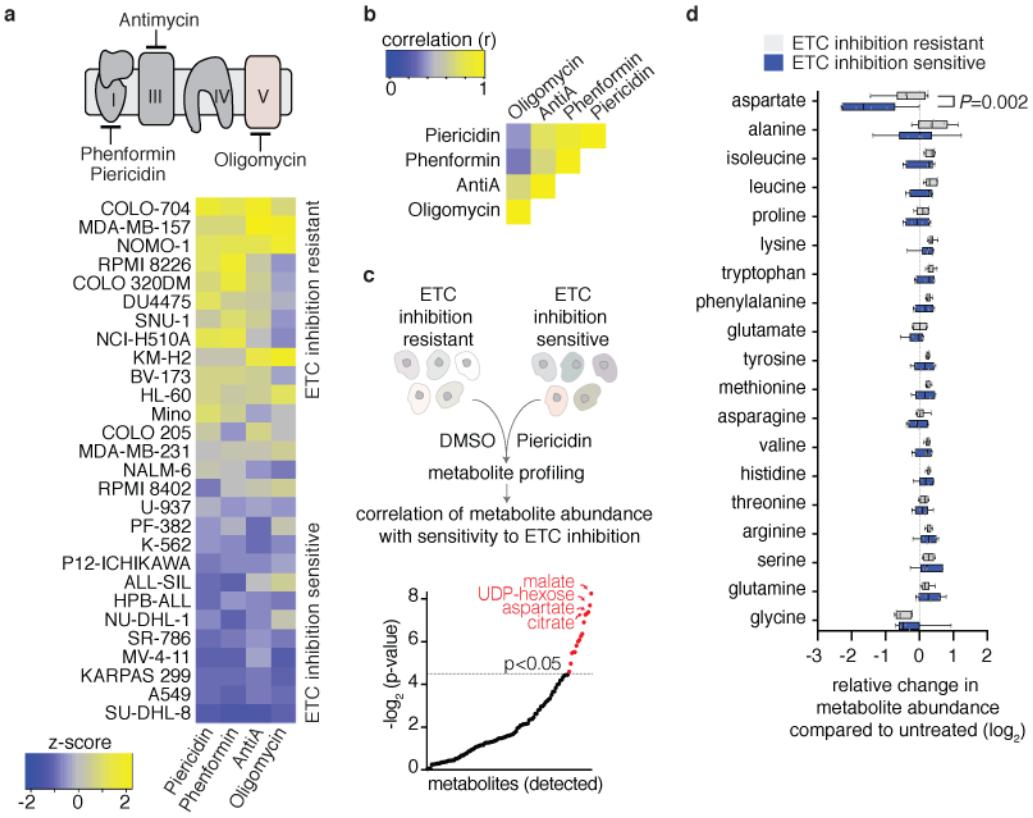

Figure 1. Diversity of cancer metabolic responses to ETC inhibition

A) Proliferation of 28 cancer cell lines treated with electron transport chain inhibitors. Graphical scheme depicting the targets of complex I (100 uM phenformin, 10 nM piericidin), complex III (30 nM antimycin A) and complex V (100 nM oligomycin) (top). Heat map indicating the changes in cell numbers upon treatment with ETC inhibitors as calculated z-scores (bottom).

B) Correlation of the sensitivities of 28 cancer cell lines to different ETC inhibitors. n=3 biologically independent samples per cell line.

C) Metabolites significantly altered between ETC inhibition resistant and sensitive cell lines upon 8 h piericidin (10 nM) treatment, ranked by p-value($-\log_2$ transformed).

D) The change ($\log_2$) in amino acid abundance of ETC inhibition resistant and sensitive cell lines upon piericidin (10 nM) treatment (The boxes represent the median, and the first and third quartiles, and the whiskers represent the minimum and maximum of all data points. *P* =0.002). For each experiment, 6 ETC inhibition resistant and 6 sensitive cell lines were used. n=3 biologically independent samples per cell line. Statistics: two-tailed unpaired *t*-test. For individual *P* values, see Supplementary Table 1. Statistics source data are provided in Supplementary Table 1.

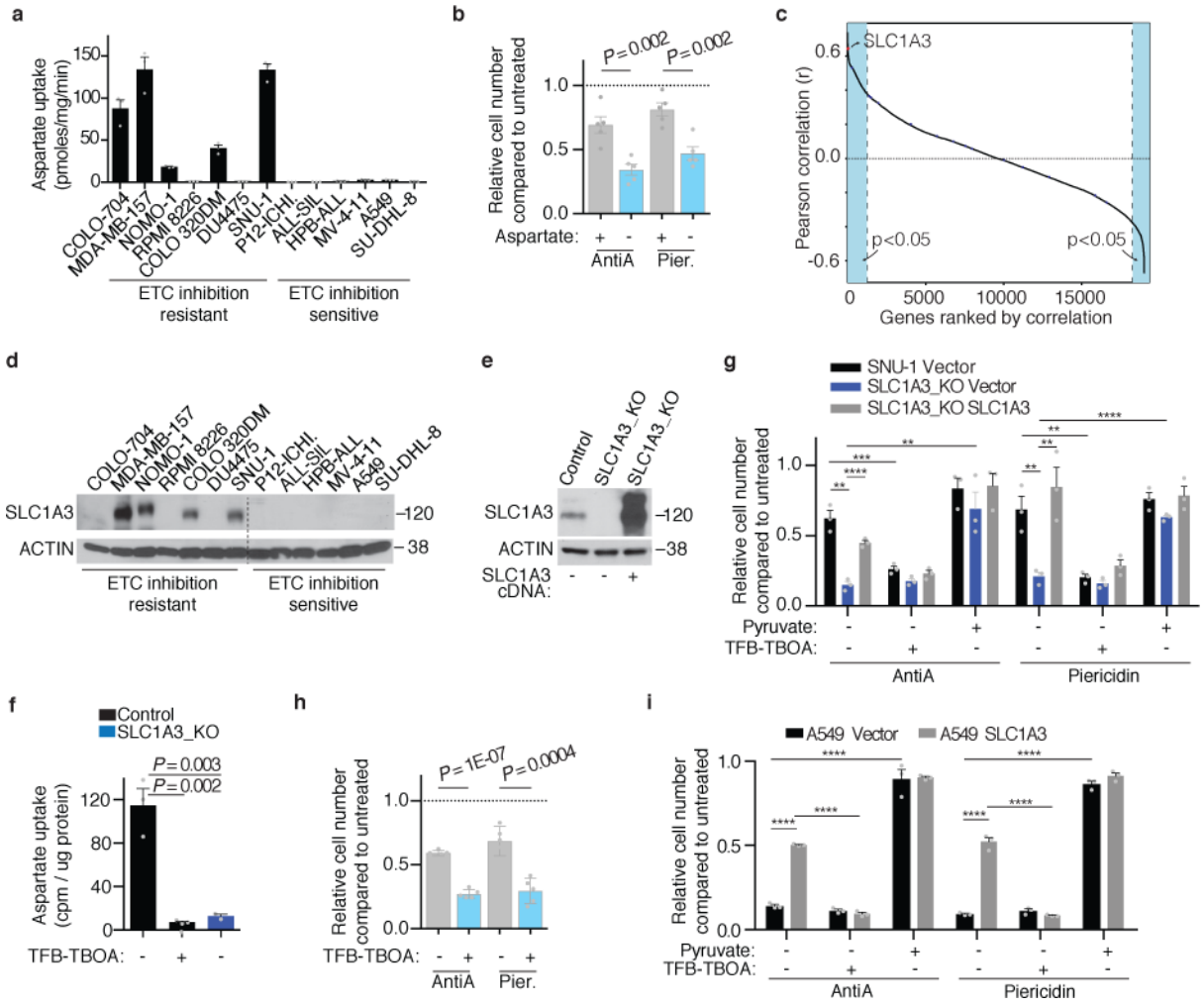

Figure 2. Aspartate import underlies the resistance of cancer cells to ETC inhibition

A) ^{14}C-Aspartate uptake in ETC inhibition resistant and sensitive cancer cell lines. (mean ± S.E.M., n=3 biologically independent samples).

B) Aspartate depletion sensitizes aspartate importing cancer cell lines to ETC inhibitors. L-Aspartate (150 uM), antimycin (30 nM) and piericidin (10 nM) were added where indicated. (mean ± S.E.M., 5 cell lines in each group, n=3 biologically independent samples.)

C) Correlation of the sensitivities to ETC inhibitors with transcriptome-wide mRNA expression data from the Cancer Cell Line Encyclopedia (CCLE). The resulting Pearson correlation coefficients were sorted and plotted. The red dot indicates *SLC1A3.* (n=28 cell lines from Fig. 1A).

D) Immunoblot analysis of SLC1A3 in ETC inhibition resistant and sensitive cell lines. Actin, loading control.

E) Immunoblot analysis of SLC1A3 in wild-type, SLC1A3-null, and rescued null SNU-1 cells. Actin, loading control.

F) ^{14}C-Aspartate uptake in wild type, SLC1A3 null and SNU-1 cells treated with an SLC1A3 inhibitor (TFB-TBOA, 20 uM). (mean ± S.E.M., n = 3 biologically independent samples).

G) Loss of SLC1A3 sensitizes cancer cells to antimycin and piericidin in RPMI. Relative cell number of wild-type (black), SLC1A3-null (blue) and rescued SLC1A3-null (gray) SNU-1 cells in the absence and presence of pyruvate (1 mM) or TFB-TBOA (20 uM) after treatment with piericidin (10 nM) and antimycin (30 nM) for 5 days. (mean ± S.E.M., n=3 biologically independent samples).

H) Pharmacologic inhibition of SLC1A3 sensitizes aspartate importing cancer cell lines to antimycin (30 nM) and piericidin (10 nM). Cells were grown for 5 days in the absence or presence of TFB-TBOA (20 uM). (mean ± S.D., 5 cell lines in each group, n=3 biologically independent samples).

I) Expression of SLC1A3 rescues A549 from the anti-proliferative effects of antimycin and piericidin in standard RPMI media, which contains 150 uM aspartate. Relative cell number of control (black), and SLC1A3 overexpressing (gray) A549 cells in the absence and presence of pyruvate (1 mM) or TFB-TBOA (20 uM) after treatment with piericidin (10 nM) and antimycin (30 nM) for 5 days. (mean ± S.E.M, n=3 biologically independent samples). Statistics: two-tailed unpaired *t*-test. For individual *P* values, see Supplementary Table 1. Statistics source data are provided in Supplementary Table 1.

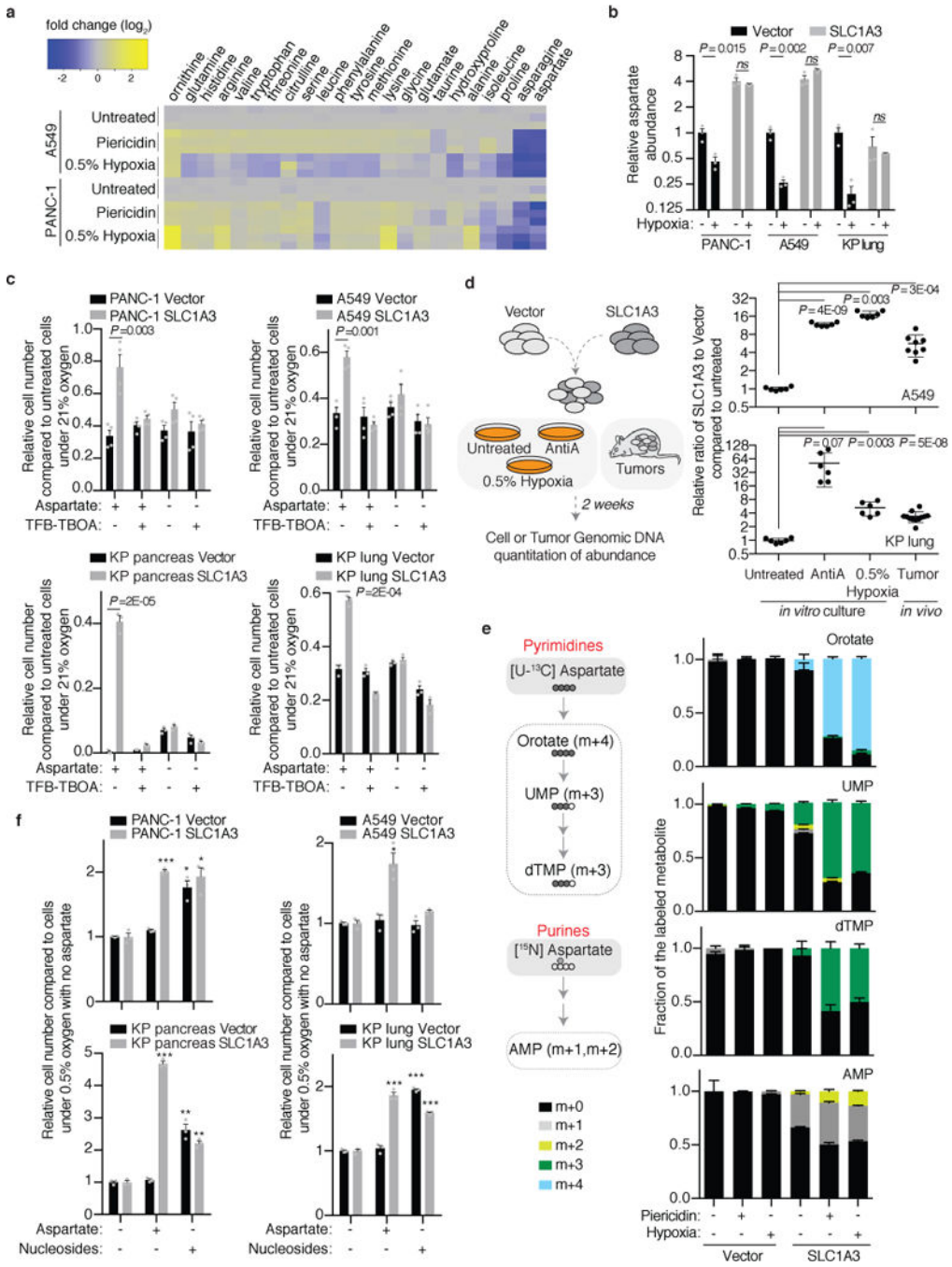

Figure 3. Aspartate is a limiting metabolite for cancer cell proliferation under hypoxia and in tumors

A) Differential intracellular amino acid abundances (log_2) of A549 and PANC-1 cells upon piericidin (10 nM) treatment or under 0.5% oxygen, relative to untreated control cells under 21% oxygen. The cells were cultured in RPMI media without glutamate and asparagine. **B)** Aspartate abundance in control (Vector, black) and SLC1A3 expressing (SLC1A3, gray) cell lines under hypoxia, relative to controls under 21% oxygen. (mean ± S.E.M, n=3 biologically independent samples).

C) Relative cell number of control (Vector) or SLC1A3 overexpressing (SLC1A3) cell lines under 21% and 0.5% oxygen with or without supplementation of aspartate (150 uM) and TFB-TBOA (20 uM). The cells were cultured in RPMI media without aspartate, glutamate and asparagine. KP lung and pancreas indicates $Kras^{G12D}/p53^{-/-}$ mouse cancer cell lines. (mean ± S.E.M., n=4 biologically independent samples for PANC-1 and A549, 3 biologically independent samples for KP lines).

D) General scheme of the cancer cell competition experiment (left). Relative abundance of A549 and Kras/p53 lung cancer cells transduced with a control vector or with SLC1A3 cDNA grown *in vivo* as xenografts or *in vitro* under antimycin (30 nM) treatment or 0.5% oxygen (right). Results are plotted relative to untreated cells under 21% oxygen. (mean ± S.E.M, n=6 biologically independent samples for *in vitro* conditions, n=8 biologically independent samples for A549 tumors, n=14 biologically independent samples for KP Lung tumors).

E) Schematic depicting the metabolic routes of aspartate in pyrimidine and purine synthesis. Filled circles represent ^{13}C or ^{15}N atoms derived from [U-^{13}C]-L-aspartate or [^{15}N]-L-Aspartate (left). Fraction of labeled nucleotide precursors derived from labeled aspartate in control and SLC1A3 overexpressing A549 cells cultured for 24 hr with [U-^{13}C]-L-Aspartate (150 uM) or [^{15}N]-L-Aspartate (150 uM) upon piericidin treatment (10 nM) or under 0.5% oxygen. Colors indicate mass isotopomers (mean ± S.D., n=3 biologically independent samples) (right).

F) Relative cell number of control (Vector) or SLC1A3 overexpressing (SLC1A3) cell lines under 0.5% oxygen with or without supplementation of aspartate (150 uM) or nucleosides (thymidine, uridine, adenosine, cytidine and inosine; 100 uM). The cells were cultured in RPMI media without aspartate, glutamate and asparagine. KP lung and pancreas indicates $Kras^{G12D}/p53^{-/-}$ mouse cancer cell lines. Results are plotted relative to cells cultured under 0.5% oxygen without aspartate or nucleoside supplementation. (mean ± S.E.M., n=3 biologically independent samples, *p < 0.01, **p < 0.001, ***p < 0.0001).

Statistics: two-tailed unpaired *t*-test. For individual exact *P* values, see Supplementary Table 1. Statistics source data are provided in Supplementary Table 1.

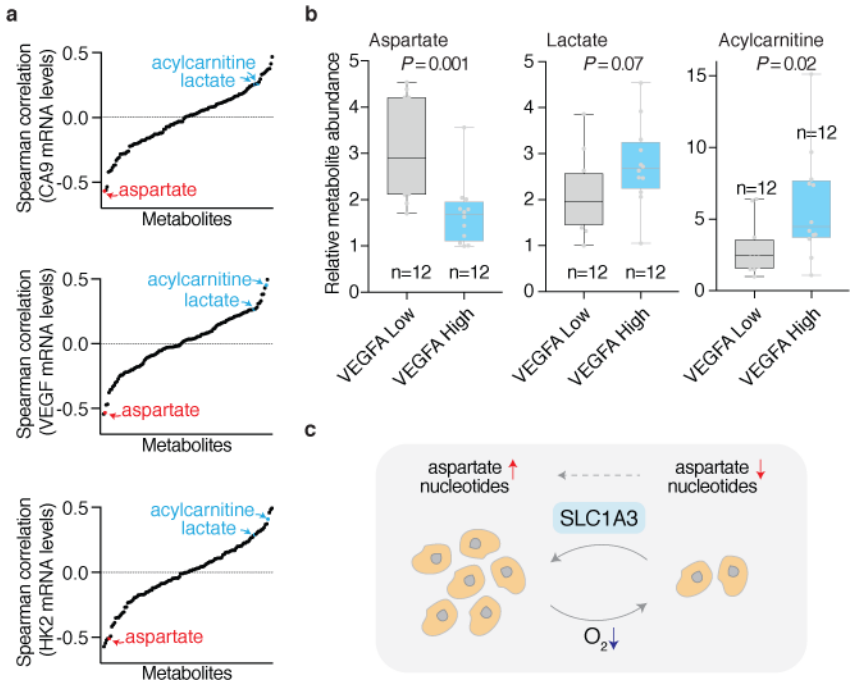

Figure 4. Aspartate levels inversely correlate with the expression of hypoxia-induced genes in primary human tumors

A) Correlation of 128 metabolites and hypoxia induced mRNA markers (CA9, VEGF and HK2) in 24 human glioblastoma tumors.

B) Relative aspartate, lactate and acyl-carnitine levels in VEGF high (n=12 biologically independent samples) and low (n=12 biologically independent samples) tumors to population minimum. The boxes represent the median, and the first and third quartiles, and the whiskers represent the minimum and maximum of all data points. Statistics: two-tailed unpaired *t*-test.

C) Proposed mechanism of the limiting role of aspartate in cell proliferation under tumor hypoxia.